Nafar Dastgerdi, J.; Anbarlooie, B.; Miettinen, A.; Hosseini-Toudeshky, H.; Remes, H.

Effects of particle clustering on the plastic deformation and damage initiation of particulate reinforced composite utilizing X-ray CT data and finite element modeling

Published in:
Composites Part B: Engineering

DOI:
10.1016/j.compositesb.2018.07.027

Published: 15/11/2018

Document Version
Peer-reviewed accepted author manuscript, also known as Final accepted manuscript or Post-print

Effects of particle clustering on the plastic deformation and damage initiation of particulate reinforced composite utilizing X-ray CT data and finite element modeling

[a,b]J. Nafar Dastgerdi, [b]B. Anbarlooie, [c,d]A. Miettinen, [b]H. Hosseini-Toudeshky, [a]H. Remes

[a] Department of Mechanical Engineering, Aalto University school of Engineering, P.O. Box 14300, FIN-00076 Aalto (Espoo), Finland

[b] Department of Aerospace Engineering, Amirkabir University of Technology, 424 Hafez Avenue, Tehran, Iran

[c] Department of Physics, University of Jyvaskyla, P.O. Box 35, Jyvaskyla, FIN-40014, Finland

[d] Swiss Light Source, Paul Scherrer Institute, Villigen, CH-5234, Switzerland

[a]jairan.nafardastgerdi@aalto.fi

Abstract

In this paper, a new simulation technique which can include microstructural inhomogeneity of particulate reinforced composites is proposed to accurately study deformation pattern and damage mechanism in these composites. Three dimensional microstructures constructed from XCT images incorporated into finite element modeling codes with minimal approximation to capture the effects of cluster size, local volume fraction of particles in the cluster and the distance between clusters as relevant statistical quantities describing the microstructural inhomogeneity of particulate reinforced composites. A quantitative parameter as degree of clustering is defined to consider particle clustering effect. The results indicate that the damage growth rate of composite with higher degree of clustering is significantly higher than those composites with lower degree of clustering. It is found that for region with higher degree of clustering and bigger size of clusters, the von Mises stress is higher at the same loading condition and the growth rate of plastic flow is considerably

higher than the other region with lower degree of clustering. Moreover, the dislocation description of deformation in two-phase materials rationalize particle clustering effect on the yield behavior of the particulate reinforced composites and the flow stress in these composites. The macroscopic stresses that lead to the initial yielding in the matrix decrease when clusters closely proximate with bigger size and higher degree of clustering.

Keywords: A. Particle-reinforcement, B. Plastic deformation, C. Finite element analysis (FEA), D. Non-destructive testing

1. Introduction

A thorough understanding of how a heterogeneous material's microstructure affects its macroscopic properties is of great importance in design and development of high performance heterogeneous materials. This is particularly challenging given the multiphase and heterogeneous nature of most high-performance composites. Modeling and prediction of the overall elastic–plastic response and local damage mechanisms in heterogeneous materials, in particular particle-reinforced composites, is a very complex problem. Various theoretical and numerical methods are proposed to clarify the relationship of the microstructure and the macroscopic property, of which the finite element (FE) analysis is an important effective method [1-6]. The FE analysis primarily requires the development of methods to automatically generate geometrical or mesh models to actually take into account complex microstructures of heterogeneous materials. However, due to the very irregular shape and complex distribution of phases, the incorporation of the information about microstructures into the models is one of the challenges in computational mechanics [7].

Finite element method (FEM)-based models are often applied to the so called representative volume element (RVE), thus assuming that the microstructure of the composite can be reproduced by assembling a large number of such elements. However, this can be a serious limitation when dealing with complex and highly heterogeneous composites microstructures, such as randomly dispersed particulate systems. Therefore, an approach able to consider the actual microstructure of the composite is useful in order to accurately predict the overall properties. The RVE models have been developed from the simplest two dimensional (2D) versions, which assume rather specific shape and distribution of phases, to complex three dimensional (3D) models, which take into account most characteristics of the real shape and distribution of material components [8-12].

Recent developments in high-resolution 3D imaging techniques, such as focus ion beam (FIB)/scanning electron microscopy (SEM) or X-ray computed tomography (XCT) launched a larger interest in performing 3D simulations on the actual microstructure of different materials [13-22]. The combination of XCT and image analysis proved to be a powerful tool to characterize heterogeneous material's microstructure in 3D, providing information that cannot be obtained with traditional 2D microscopy techniques. XCT has been used as a basis for obtaining microstructurally realistic FE models. XCT has ability to detect the internal structure as small as 1 μm, which provides a feasible method to build models based on actual microstructure [23-32]. These models considering the inherent morphology, clustering and arrangement of phases, with minimal microstructural approximations, are frequently adopted to analyze the macroscopic behaviors of heterogeneous materials.

Chawla and co-workers [33] have shown that 3D microstructures constructed from serial sectioning can be incorporated into commercial FEM codes to model the deformation behavior of composites. Maire *et al* [34] discussed different possible methods for using tomography results as

inputs for numerical models, especially FE meshes. They classified three different ways to produce meshes reflecting the actual architecture of a cellular material: meshes generated from a Voroni description of microstructure, voxel/element meshes, and tetrahedral meshes of the actual shape of the cellular architecture. Yu et al [35] proposed a method to identify micro scale fiber bundle configuration of a needle-punched carbon-carbon composite through micro-CT image processing. Then a FE model is built and used to predict mechanical properties and simulate progressive damage of this composite. Li et al [36] used both the micro-CT observations and FE analyses to investigate the impact shear damage mechanisms and energy absorption of the 3D braided composite.

It has been shown that the mechanical behavior and properties of particulate reinforced composites are highly dependent on the real microstructure of the composite and particle distribution and volume fraction. In most particulate reinforced composites, the particles are not uniformly distributed. Instead, these materials contain local regions where the particles are clustered. It is well established experimentally that damage nucleation in polymer- and metal-matrix composites occurs in regions of the microstructure that contain high local volume fraction of reinforcements [37-41]. Thus, the accurate simulation of deformation and damage initiation in composites requires new simulation techniques which can include inhomogeneous reinforcement distributions.

In this study, the effects of clustering and critical microstructural characteristics of particulate reinforced composite on deformation pattern and damage mechanism have been investigated using 3D FE modeling. Quantitative analysis of the critical characteristics with regard to the effect of particle clustering have been obtained using XCT data in the first part of this study [42]. The relevant statistical quantities describing the microstructural inhomogeneity of particulate reinforced composites ($Ni_{60}Nb_{40}$/Mg) have been used as input for FE modeling with minimal

microstructural approximation. The proposed new simulation technique can include microstructural inhomogeneity of particulate reinforced composites to accurately study deformation pattern and damage mechanism in these composites using XCT data incorporated into FE models. Moreover, particle-clustering effect on yield behavior and flow stress of these composites has been qualitatively studied using dislocation description of deformation in two-phase materials.

2. Materials and methods

2.1. Materials

Amorphous alloy powder with composition $Ni_{60}Nb_{40}$ (at. %) was prepared by mechanically alloying powder mixtures of elemental Ni and Nb metals. The powder mixture was milled at room temperature in air for 87 h, using a Retsch PM400 planetary ball mill with a ball-to-powder ratio of 3:1 and milling speed of 200 rpm. To produce Mg-composites, elemental Mg-powder (99.6% purity) was blended with volume fraction 5% of $Ni_{60}Nb_{40}$ powder for a duration of 1 h and consolidated at room temperature at 450 MPa for 1 min. The compacted cylindrical billets of 36 mm diameter were microwave sintered at 100% power level for 12.5 min so as to achieve a temperature of 550^0C (based on prior calibration). The sintered billets were soaked at 400^0C for 1 h, and hot extruded at 350^0C to produce rods of 8 mm diameter. Rods extruded at 750 psi and 600 psi were used for further analysis.

2.2. Microstructural characteristics using X-ray microtomography

In order to understand the mechanical behavior of particulate reinforced composites, it is important to investigate the size, morphological characteristics, and distribution of inclusions in the material. If a group of reinforcement particles is closely packed such that the mechanical properties of the material near the particle group differ from the surroundings, the particle group is referred to as a

"cluster" [6]. In the following, XCT imaging is used to provide a precise picture of the microstructural heterogeneity and clustering in these composites.

For high-resolution XCT imaging a cylindrical (diameter ≈ 1 mm, height ≈ 1 mm) region was selected from the rod sample. According to the measuring procedure introduced in [42], the sample was imaged using Xradia MicroXCT-400 tomograph (Zeiss Xradia, Concord, California, USA) with 0.59 μm pixel size. The X-ray tube voltage and power were 40 kV and 4 W, respectively, and a 0.37 mm glass filter was applied. Total of 1800 projection images over 360 degrees of rotation were acquired with 50 s exposure time per angular position. The projection images were reconstructed using utility software provided by the manufacturer of the tomograph, resulting in a 3D volume image where the pixel values are roughly proportional to the local X-ray attenuation coefficient [43]. In order to characterize the clustering based on the reconstructed images, the reinforcement regions shown in the image (Fig. 1a) must be classified into individual particles and clusters. Comparison of the reconstructed images to, e.g., scanning electron microscope images of similar clustered material (Fig. 1b) suggests that the resolution of the reconstructed images is not high enough to fully differentiate individual particles inside particle clusters, but individual clusters are easily differentiated from each other [42]. The clusters are shown in the images as large connected reinforcement regions with varying X-ray attenuation coefficient. As the images show the individual particles inside the clusters mostly connected to each other, geometrical conditions like distance of individual particles are not effective for classification purposes. Instead, a condition based on the local X-ray attenuation coefficients inside each reinforcement region was used, as described below.

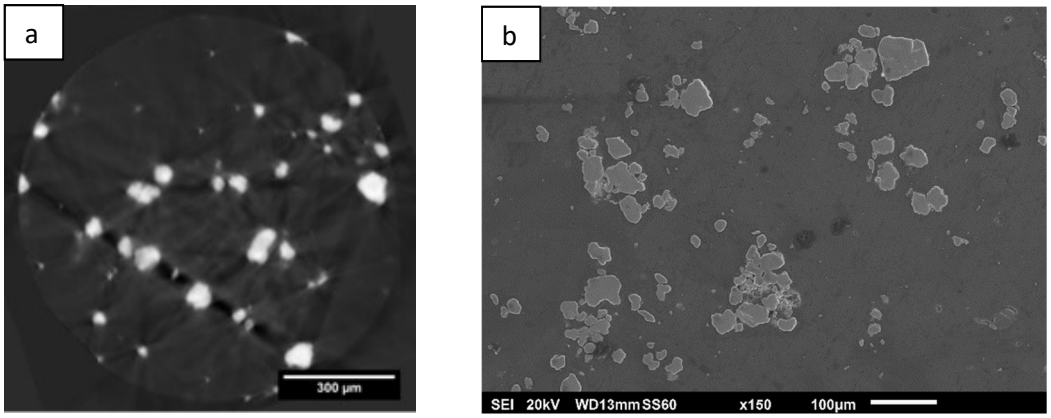

Fig. 1. (a) Slice through a high-resolution XCT image of the sample extruded at 600 psi and (b) SEM image with internal inhomogeneous distribution for similar sample.

To facilitate the classification, the reinforcement regions were segmented using the Phansalkar method [43]. The segmented regions were classified into clustered and individual particles based on observation that a cluster consisting of multiple smaller particles has many local X-ray attenuation coefficient maxima inside it, each of the maxima roughly originating from a single reinforcement particle inside the cluster. The count of local maxima was determined for each particle and reinforcement regions with more than three maxima were classified as clusters. All other particles were classified as individual reinforcement particles. This classification process resulted in a visually plausible result as shown in Fig.2a-b for two specimens chosen from different rods extruded at 600 psi and 750 psi, respectively.

The amount of clustering can be naturally expressed by dividing the total volume of particles V_f into two parts V_f^c and V_f^m where V_f^c is the volume of clustered particles, V_f^m is the volume of individual particles, and $V_f = V_f^c + V_f^m$. The degree of particle clustering in particulate reinforced composites quantitatively describe as follows:

$$\zeta = \frac{V_f^c}{V_f} \tag{1}$$

where ζ is the volume ratio of clustered particles over the total particles in the matrix.

For a composite, the volume fraction of particles f_1 is defined by:

$$f_1 = \frac{V_f}{V} \tag{2}$$

Where V is volume of composite. Denote f_1^c as volume fraction of particles agglomerated in the cluster regions and f_1^m volume fraction of individual particles in the matrix. We can give the relationships of f_1, f_1^c and f_1^m versus the degree of clustering, ζ, as below:

$$f_1^c = \frac{V_f^c}{V} = f_1\zeta, f_1^m = \frac{V_f^m}{V} = f_1(1-\zeta) \tag{3}$$

Two types of 5 vol. % $Ni_{60}Nb_{40}$/Mg composites with different microstructure and degree of particle clustering were studied in this work to highlight the capability of the proposed new simulation technique which can include microstructural inhomogeneity of particulate reinforced composites. Based on the proposed definition, the clustering parameter,ζ are respectively 0.9 and 0.51 for these composites. This means that for composite extruded at lower extrusion pressure, around 90% of the particles are agglomerated in the clustered regions and 10% of particles are uniformly dispersed in the matrix. While for composite extruded at higher extrusion pressure, around 51% of the particles are clustered and 49% of particles are found as individual particles in the matrix.

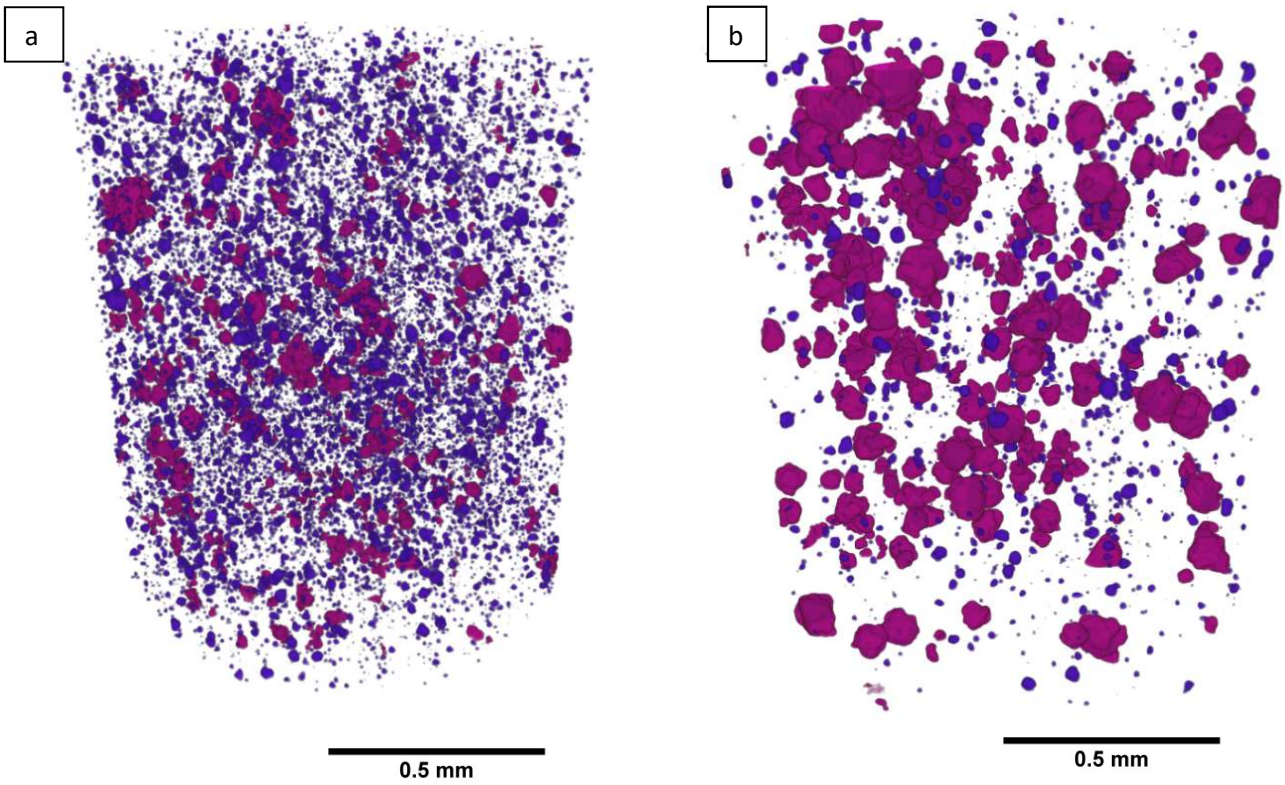

Fig. 2. 3D visualizations of different types of composite microstructure extruded at (a) 750 psi and (b) 600 psi, respectively. Red and purple colors correspond to clustered and individual particles, respectively.

2.3. Microstructure-based finite element modeling

In order to make the model closer to reality, 3D RVE should be generated on the basis of real microstructure of the samples. It is necessary to find first the cluster spatial coordinates that describe the real spatial distribution of clusters in the matrix. Firstly, the bounding sphere for each cluster, i.e. the smallest sphere that contains all the cluster pixels, was determined using Welzl method [45] that calculates the optimal bounding sphere of a set of points in linear time using a randomized linear programming type algorithm. Thus, the spatial coordinates of clusters are determined in the samples based on the center coordinates of the bounding sphere for each cluster. Secondly, the equivalent spherical diameter, d_{eq} (Fig. 3), was determined, which equals the diameter of sphere having the same volume of individual cluster, V_f^{ci} , as described in Eq. (2).

$$d_{eq} = (\frac{6}{\pi} V_f^{ci})^{\frac{1}{3}} \quad (2)$$

V_f^{ci} is determined as total count of pixels for each individual cluster.

Fig. 3. Bounding sphere diameter ($d_{bounding}$) and equivalent spherical diameter of cluster (d_{eq}).

Figure 4a-b shows the normal and log- normal probability distribution of the equivalent spherical diameter and bounding sphere diameter for sample extruded at different extrusion pressure. The equivalent spherical diameter distribution has closely the same bounding sphere diameter distribution. However, the differences between the equivalent spherical diameter and bounding sphere diameter for sample extruded at higher pressure with lower concentration of cluster regions are higher. It should be noted that the diameter of the bounding sphere for each cluster describes the maximum extension of the cluster; therefore, these results reveal clusters have different morphology related to various extrusion pressure. This is correlated with results obtained in previous study using X-ray nanotomography that suggested there may be two types of clusters in the present composites; relatively spherical ones for sample extruded at lower pressure and more ellipsoidal ones for sample extruded at higher pressure [42].

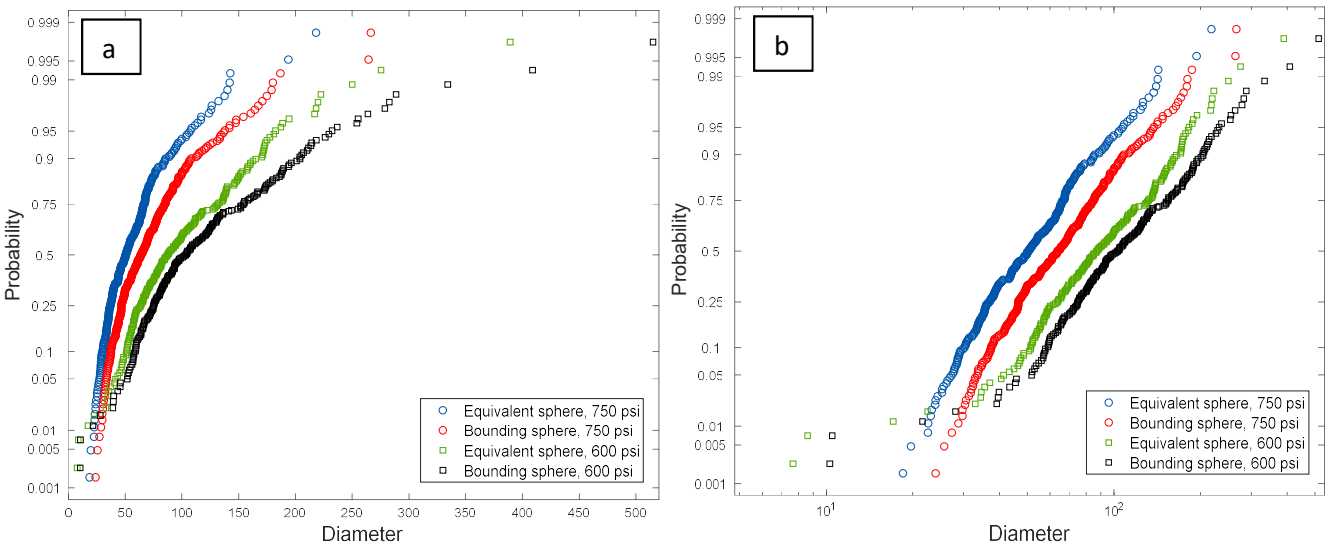

Fig. 4. (a) Normal, and (b) log- normal probability distribution of the equivalent spherical diameter and bounding sphere diameter for sample extruded at 750 psi and 600 psi.

In Fig. 5a-b, the equivalent spherical diameter, d_{eq}, is compared to the bounding sphere diameter for sample extruded at 600 psi and 750 psi, respectively. The comparison reveals an approximately linear behavior, but exhibits enhanced scatter in larger cluster sizes. For further modeling and analyses in this study, the equivalent spherical diameter, d_{eq}, was employed due to the proportionality of d_{eq} and the bounding sphere diameter, which leads to acceptable results for statistical examination and modeling. These microstructural data sets can be incorporated into FE models to predict the onset of local damage mechanisms and the deformation pattern of particulate reinforced composites.

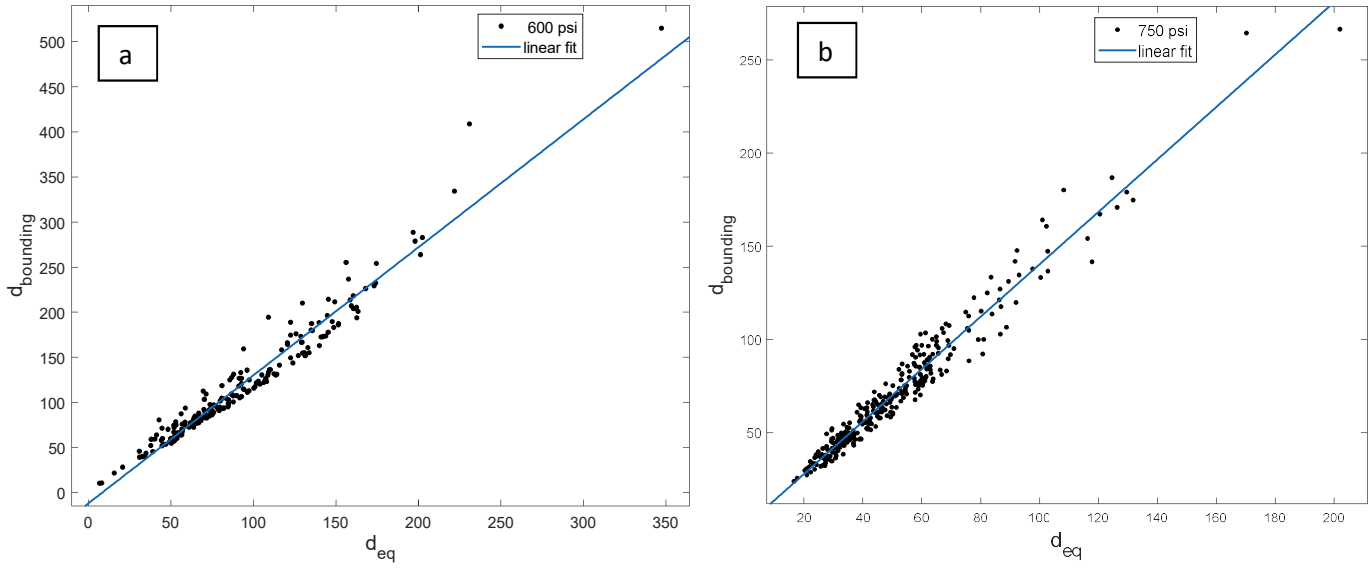

Fig. 5. The equivalent spherical diameter, d_{eq}, over the bounding sphere diameter for sample extruded at (a) 600 psi and (b) 750 psi.

On the basis of bounding spheres and equivalent diameter of clusters, two RVEs representing clusters in 3D microstructure of Fig. 2a-b were constructed as depicted in Fig. 6 a-b. Two sub-RVEs have been extracted from the whole RVE for composites with different extrusion pressure. These typical RVEs are chosen from the center of the whole RVE. The selected RVEs contain the equivalent clusters while in order to define RVEs based on the real microstructure of the composites in each case the individual particles should be added to the RVEs. This addition of individual particles to each RVE occurred based on the value of proposed clustering parameter, ζ, and f_1^m, as presented in section 2.2. Thus, Fig. 6c-d shows the finite element RVEs generated for 3D microstructure of Fig. 2a-b on the basis of real microstructure of particulate reinforced composite with minimal microstructural approximation. This approach is applicable for different type of particulate reinforced composite materials. In this paper, two types of 5 vol. % $Ni_{60}Nb_{40}$/Mg composites with different microstructure and degree of particle clustering were studied to highlight the capability of the proposed new simulation technique which can include microstructural

inhomogeneity of particulate reinforced composites using XCT data as input for FE modeling with minimal microstructural approximation.

The material properties of the composite constituents are presented in Table 1. The Young's modulus of the $Ni_{60}Nb_{40}$ amorphous particles is measured by nanoindentation method. In the composite medium, the matrix undergoes elastic-plastic deformation and the reinforcement deforms elastically. Mg matrix and the $Ni_{60}Nb_{40}$ amorphous particles are considered to behave as elasto-plastic and elastic-perfectly plastic materials, respectively. The multi-linear isotropic hardening Mises plasticity law is used for the plastic behavior of the model.

Material	$E(GPa)$	υ	$\sigma_{YS}\,(MPa)$
Pure Mg	42.29 ± 0.93	0.35	80 ± 9
$Ni_{60}Nb_{40}$	150 ± 7	0.3	-

Table 1. Material parameter of the composite constituents

A free mesh containing 3D 8 node solid element and suitable for modelling irregular meshes was used in this study to have an accurate model of microstructure. Symmetric boundary conditions are applied on three faces while constraint equation is applied to the nodes on the other two faces to have equal displacements in the Y and Z directions at all nodes and fixed in the other directions. The loading is applied in various steps in the form of displacement type on the right side of the model (displacement control solution). Loading steps strategy is a requirement to control the numerical convergence of nonlinear elastic–plastic solution.

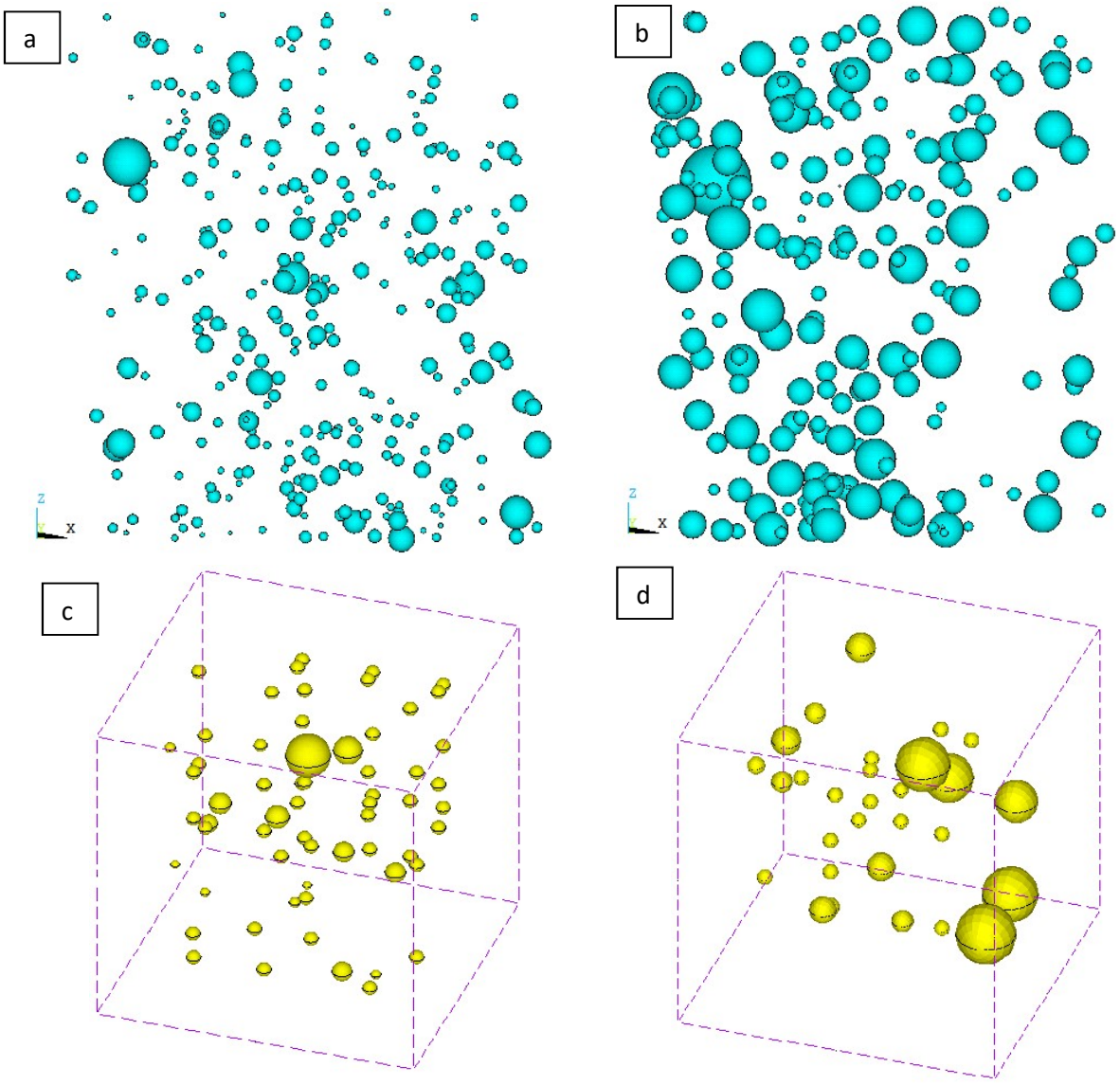

Fig. 6. RVEs generated for 3D microstructure of (a) composite extruded at 750 psi and (b) composite extruded at 600psi on the basis of real microstructure and bounding spheres and equivalent diameter of clusters. (c) and (d) sub RVEs from the center of the whole RVE for each composite.

3. Results and discussion

3.1. Particle clustering effect on plastic deformation

Figure 7a-b shows the equivalent plastic strain in the matrix at final loading step for typical RVEs presented in Fig. 6c-d, respectively. To obtain more information about particle clustering effect on plastic deformation under loading, the evolution of equivalent plastic strain, ε_{eq}, at different strain

state for composites extruded at different extrusion pressure with various degree of particle clustering is depicted in Fig. 8a-b. It can be seen that the particle clustering influences the damage behavior of composites. These histograms are obtained from plastic strain in the elements of the models. The *in-situ* growth behavior of equivalent plastic strains are depicted in Fig. 9a-d. It is found the damage growth rate of composite with higher degree of clustering is significantly higher than the other case with lower degree of clustering as shown in Fig. 9d. Moreover, the distribution of the equivalent plastic strain in the elements in the matrix, for strain state 0.1, is plotted in Fig. 10 for composites extruded at 600 psi and 750 psi, respectively. This distribution for composite with higher degree of particle clustering shows a correspondingly higher fraction of elements with lower plastic strain than the other composite with lower degree of particle clustering. The plastic deformation is constrained in the matrix regions between clusters. This distribution illustrates particle clustering has a considerable influence on the plastic flow on the matrix. It should be noted that *in-situ* growth behavior of equivalent plastic strains and histogram of the evolution of equivalent plastic strain provide more detailed information that cannot be reached by general distribution of equivalent plastic strain presented in Fig 7a-b.

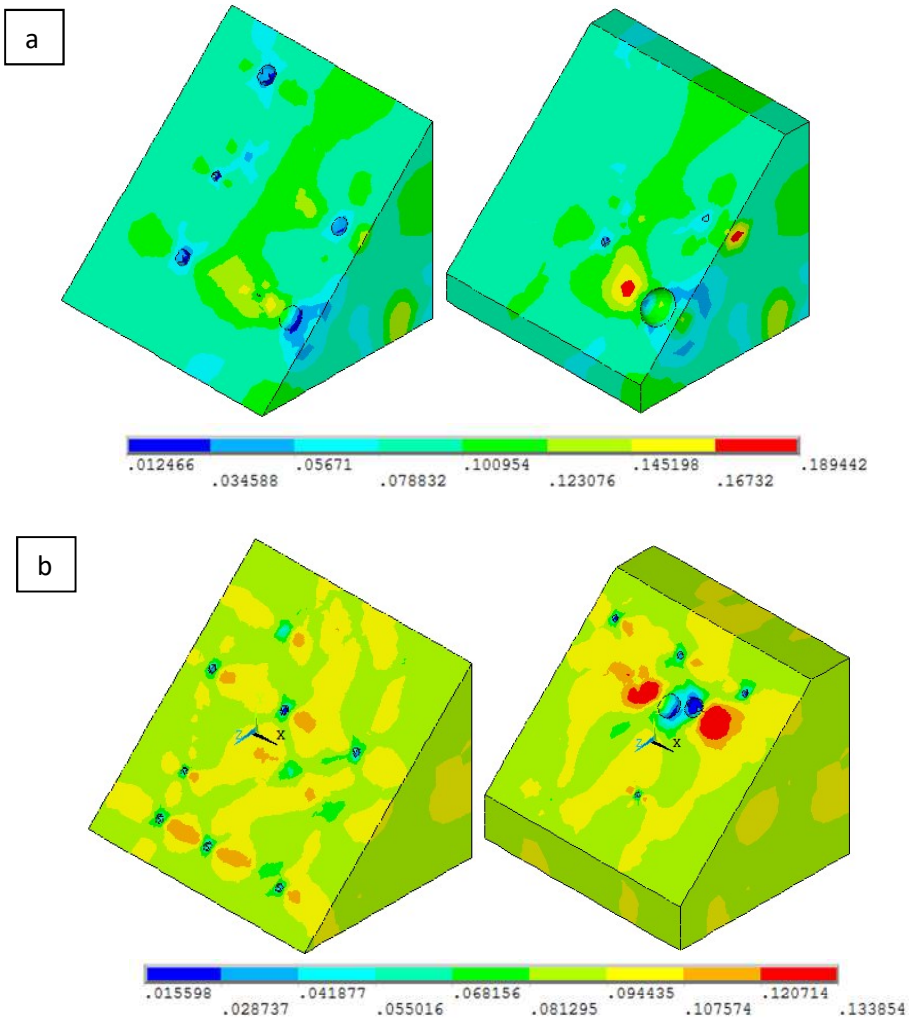

Figure 7. Equivalent plastic strain in the matrix for composite with different degree of clustering (a) $\zeta = 0.9$ and (b) $\zeta = 0.51$.

Fig. 8. The evolution of equivalent plastic strain at different strain state for composites extruded at (a) 600 psi and (b) 750 psi.

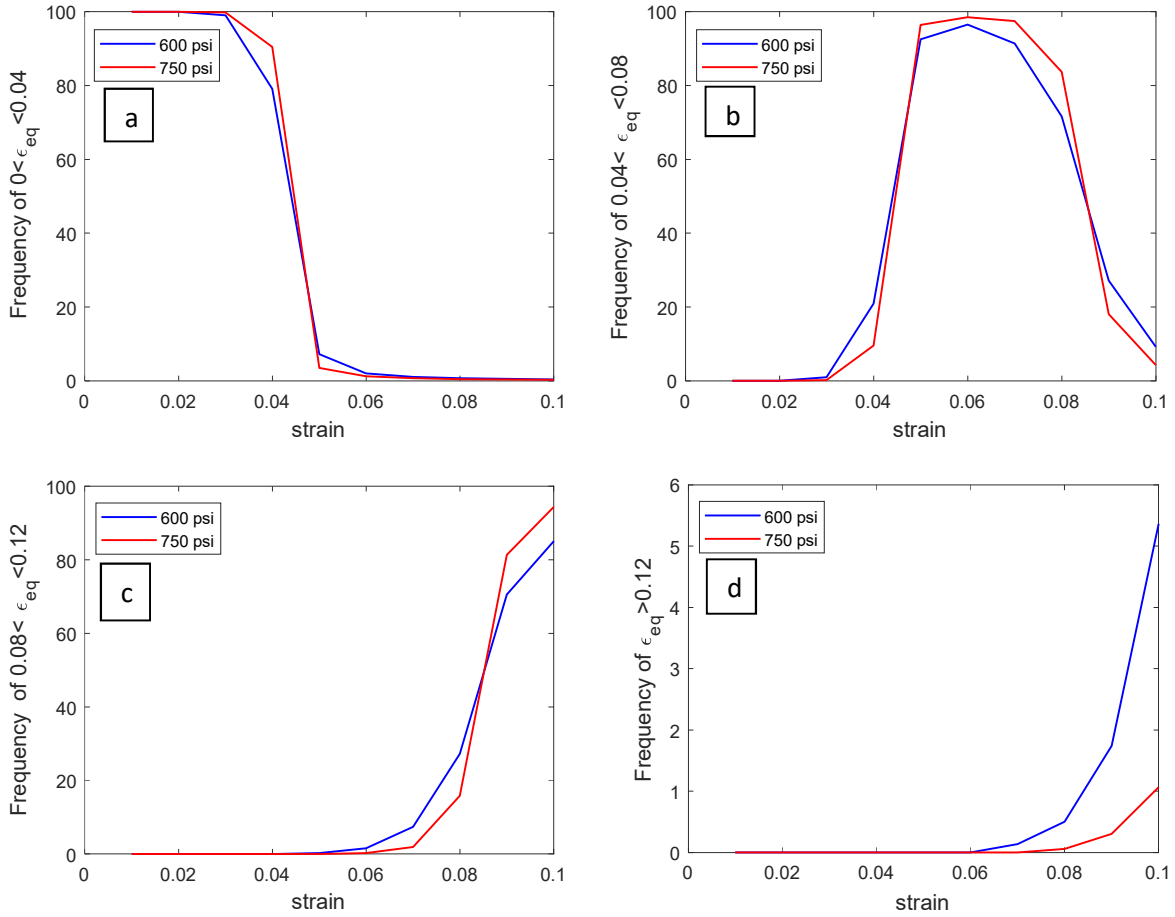

Fig. 9. (a)-(d) the in-situ growth behavior of equivalent plastic strains for composites with different degree of clustering.

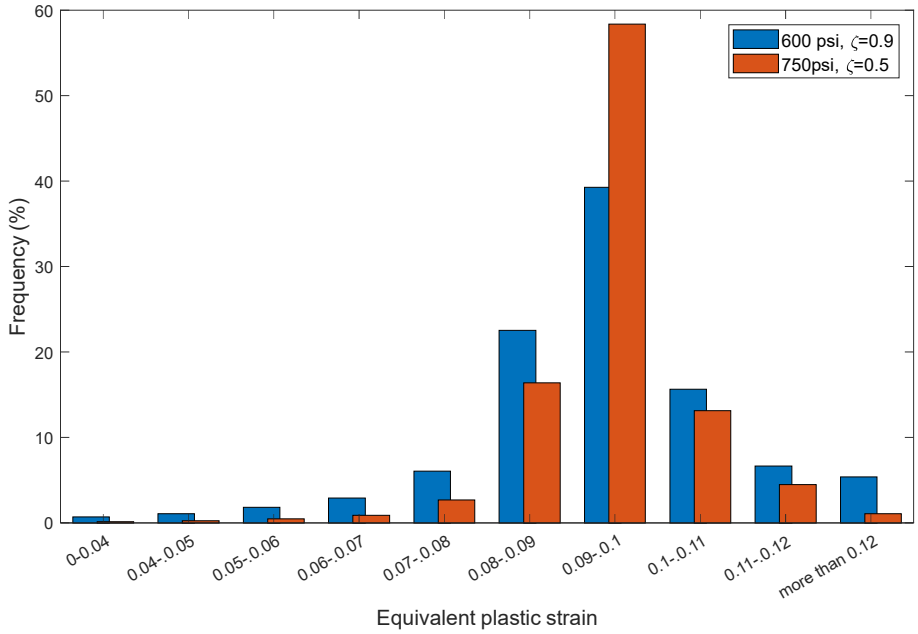

Fig. 10. Histogram of equivalent plastic strain distribution in the matrix of composites with different degree of clustering.

3.2. Particle clustering effect on flow stress and damage initiation

In two phased material such composites (or alloys), one component (often dispersed as particles in composites) deform less than the other, or not equal at all, so the gradients of deformation form with a wavelength equal to the spacing between the phases or particles. Such composites (or alloys) are plastically non-homogeneous, because gradients of plastic deformation are imposed by the microstructure. When a plastic crystal is deformed, dislocations are generated, move, and are stored; this storage causes the material to work-harden. Dislocations become stored for two main reasons: they accumulate by trapping each other, or they are required for the compatible deformation of various parts of the crystal constrained within its surroundings. The dislocations that are mutually trapped are referred to as statistically stored dislocations [46] and, as yet, there is no simple argument to estimate their density, ρ_s. The dislocations that are stored due to incompatibility in deformation are called geometrically necessary dislocations (GND), ρ_{GND}. The statistically stored dislocations is a characteristic of material, that is, of the crystal structure, shear modulus, stacking-fault energy, etc. The GND is a characteristic of the microstructure, that is, the geometric arrangement and size of phases or particles. We use the concept of GND to rationalize particle clustering effect on the yield behavior of the particulate reinforced composites and the flow stress in these composites.

Strengthening of reinforcement particles on yield strength (σ_{ym}) of particulate matrix arises due to: (i) Orowan strengthening ($\Delta\sigma_{\mathrm{Orowan}}$), the stress increase needed to move a dislocation through an array of impeding particles, (ii) stress contribution due to statistically stored dislocations introduced by the thermal expansion mismatch between the matrix and reinforcement ($\Delta\sigma_{\mathrm{CTE}}$) and (iii) generation of GND to accommodate the plastic deformation mismatch between the matrix and particles ($\Delta\sigma_{\mathrm{GND}}$) [47-51]. In this study, the stress contribution due to statistically stored

dislocations introduced by the thermal expansion mismatch between the matrix and reinforcement is neglected. The strength of a reinforced matrix is given by [47,50-51],

$$\sigma_{ym}^{r} = \sigma_{ym} + \Delta\sigma \tag{2}$$

where σ_{ym}^{r} and σ_{ym} are the yield strength of reinforced and unreinforced matrices, respectively. $\Delta\sigma$ represents increment in yields of reinforced matrix and is estimated as follows:

$$\Delta\sigma = \sqrt{\Delta\sigma_{\text{Orowan}}{}^{2} + \Delta\sigma_{\text{GND}}{}^{2}} \tag{3}$$

$\Delta\sigma_{\text{Orowan}}$, can be estimated using the following equation [51],

$$\Delta\sigma_{\text{Orowan}} = \frac{\beta\mu_m b_m}{\lambda} \tag{4}$$

where β is a constant, μ_m, b_m are the shear modulus of metal matrix and its Burgers vector. λ is the interparticle spacing of the second phase particles, which is given by

$$\lambda = D(\pi/6f)^{1/3} \tag{5}$$

where f and D are the volume fraction and the diameter of the second phase, cluster, respectively. $\Delta\sigma_{\text{GND}}$ is calculated using the following equation [52],

$$\Delta\sigma_{\text{GND}} = \alpha\mu_m b_m\sqrt{\rho_{\text{GND}}} \tag{6}$$

where α is a geometric factor and the density of GNDs can be estimated by [53]

$$\rho_{\text{GND}} \approx \frac{8\gamma_m}{b_m\lambda} \tag{7}$$

with γ_m the local shear strain in the matrix.

When the particles agglomerate in clusters, the diameter of the second phase increases. Thus, the effects of aggregation of particles as clusters on the strength of a reinforced matrix and the composite can be correlated with the decrease in the extent of Orowan and GND strengthening with increasing the cluster size as a second phase in the matrix. The results of tensile property

measurements conducted on the 5 vol. % $Ni_{60}Nb_{40}$/Mg composites extruded at different extrusion pressures under tensile loading are listed in Table 2. Experimental findings show that there is a strong relationship between strength of composite and the local volume fraction and distribution of the reinforcement particles [54]. These results are in good agreement with the dislocation description of deformation in two-phase materials rationalizing particle clustering effect on the strength and yield behavior of the particulate reinforced composites. Hence, the conclusion from this section can be a valuable result for researchers in material and manufacturing to optimize mechanical properties of composites based on the knowledge of the relationship between the microstructure and the macroscopic response.

Material	Specimen code	0.2%Offset Yield Strength (MPa)	Tensile Strength (MPa)	Elongation (%)	Reduction of Area (%)
5. vol%	600 psi	84	109	1.6	1
	750 psi	174	208	1.6	1.5

Table 2. Results of room temperature tensile testing [54]

The first part of this study reveals that the critical characteristics with regard to the effect of particle clustering are cluster size, local volume fraction of particles in the cluster and the distance between clusters [42].When multiple clustered reinforcement regions are in close proximity, they behave as a large single cluster. Thus, it is important to elucidate the effects of the proximity of clusters on the local damage initiation and flow stress of particulate reinforced composites. To study the effects of particle clustering on the yield behavior of the particulate reinforced composites and the flow stress of the matrix in these composites, the sub-RVE has been extracted from the whole RVE for composite extruded at 600 psi with the highest degree of clustering ($\zeta = 1$) as depicted in Fig. 11. This sub-RVE was chosen since the effects of the cluster size and proximity of clusters clearly were illustrated.

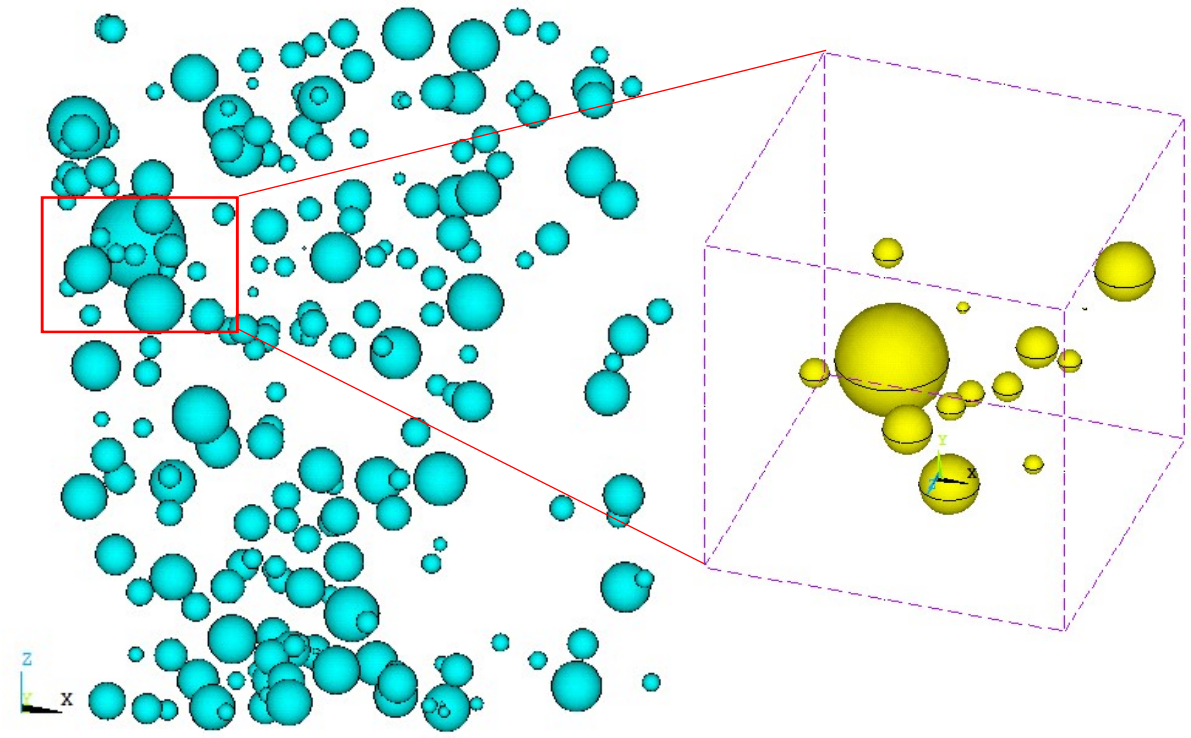

Fig. 11. Sub RVE with the highest degree of clustering extracted from composite extruded at 600 psi.

The macroscopic stresses that lead to the initial yielding in the matrix are obtained for sub-RVEs chosen from specimen extruded at 750 psi, and 600 psi with different degree of clustering based on this FEM simulation, and they are presented in Table 3.

Specimen	Macroscopic stress leading to yielding
750 psi	81.7 MPa
600 psi	72.6 MPa
600 psi, ($\zeta = 1$)	61.5 MPa

Table 3. Macroscopic stresses which lead to the initial yielding in the matrix

Figure 12a-c shows the von Mises stress distribution in the matrix at strain state 0.009 in the beginning of loading step and near to the initial yielding in the matrix for typical RVEs presented in Fig. 6c-d and Fig. 11, respectively. In this case, the frequency distribution of von Mises stress

in the matrix is depicted in Fig. 13. This figure highlight the effects of particle clustering and cluster size on the distribution of von Mises stress. It can be seen there is a uniform distribution in the case that degree of clustering and cluster size are lower as shown for composite extruded at 750 psi. In this case, around 95% of von Mises stress distributed in the interval between 70 and 80 MPa; however, for two other cases with higher degree of clustering and bigger cluster size there is not a uniform distribution. The macroscopic von Mises equivalent stress is plotted versus the non-dimensional loading time in Fig. 14. It is found that for region with higher degree of clustering and bigger size of clusters, the von Mises stress is higher at the same loading condition and the growth rate of von Mises stress is considerably higher than the other region with lower degree of clustering. The von Mises stress expresses the degree of easiness for plastic deformation. This figure implies that plastic flow on the matrix occurs earlier and easier in the case that clusters closely proximate with bigger size and higher degree of clustering.

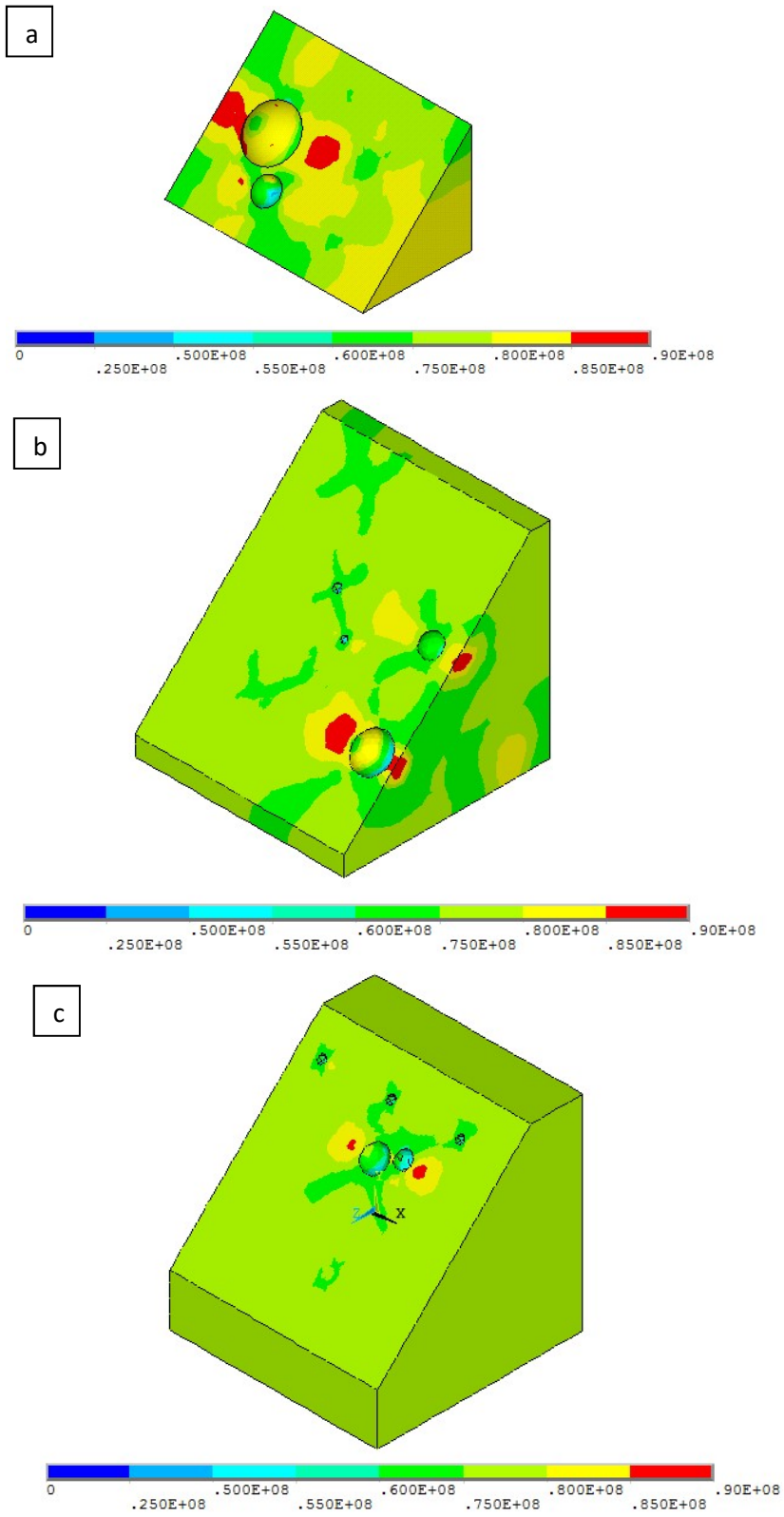

Fig. 12. Von Mises stress distribution in the matrix for composite extruded at 600 psi with different degree of clustering (a) $\zeta = 1$ and (b) $\zeta = 0.9$ and (c) for composite extruded at 750 psi with $\zeta = 0.51$.

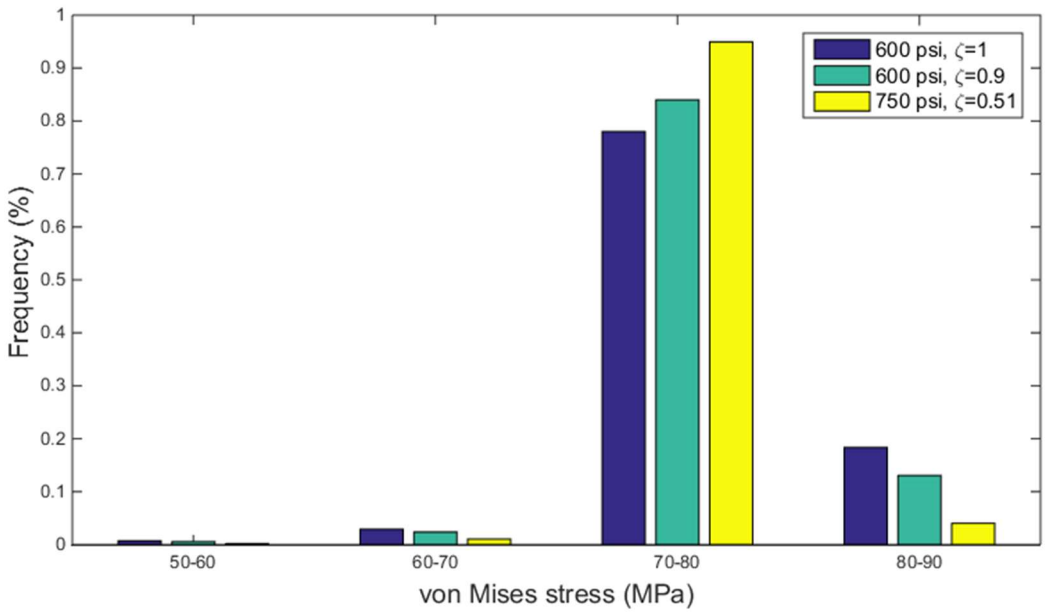

Fig. 13. Frequency distribution of von Mises stress in the matrix.

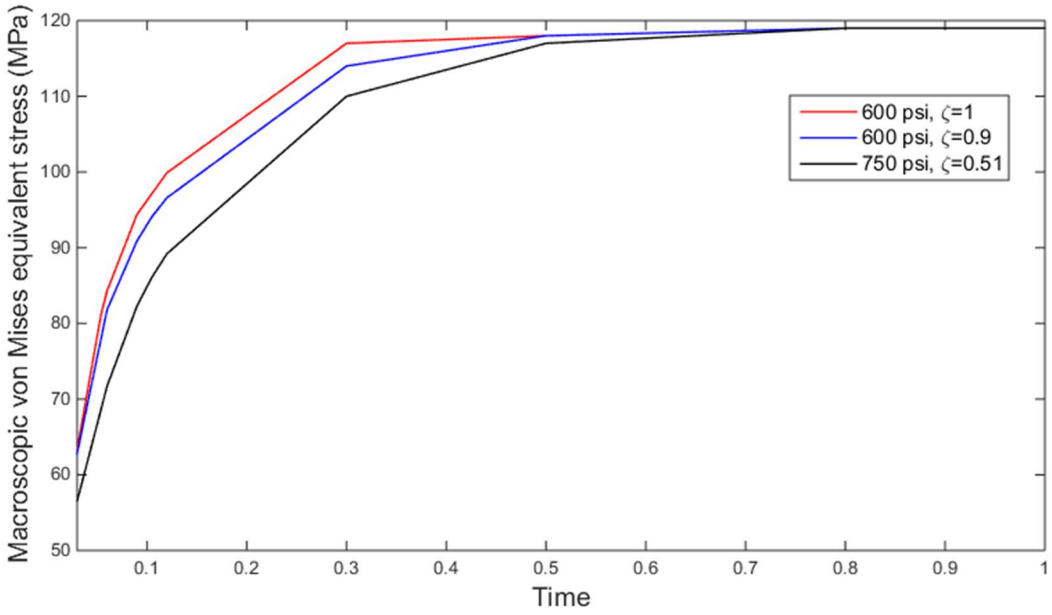

Fig. 14. The macroscopic Von Mises equivalent stress versus the non-dimensional loading time.

Moreover, the hydrostatic stress distribution of sub-RVE extracted from the composite extruded at 600 psi with the highest degree of clustering ($\zeta = 1$) is depicted in Fig. 15. It can be seen that the peak values of hydrostatic stress which are important factor for debonding and void formation happen in clusters and regions that clusters are in close proximity. As depicted in Fig. 12, the

plastic flow is prohibited in these regions and consequently by correlation with hydrostatic stress there is a great tendency towards debonding and crack initiation failure mode. It is worth to note that high level of clustering may cause some bonding problems. The clustered regions can be potential sites for void nucleation, which gives rise to earlier commencement of failure. However, this aspect should be investigated in more detail and thus the effect of clustering and critical microstructural characteristics of particulate reinforced composite on interface debonding and void formation will be further investigated in the following part of this study.

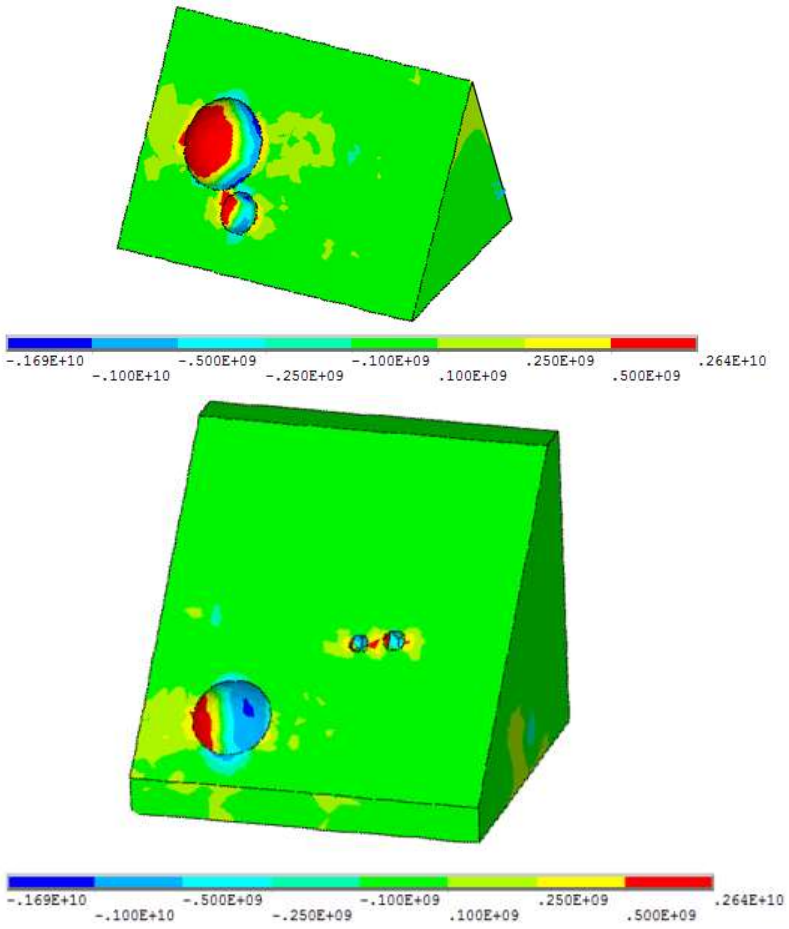

Fig. 15. The hydrostatic stress distribution of sub-RVE with the highest degree of clustering ($\zeta = 1$) for composite extruded at 600 psi.

4. Conclusions

In this study, the effects of clustering and critical microstructural characteristics of particulate reinforced composite on deformation pattern and damage mechanism have been investigated using 3D FE modeling. 3D microstructures constructed from XCT images incorporated into FEM codes with minimal approximation to capture the effects of cluster size, local volume fraction of particles in the cluster and the distance between clusters as relevant statistical quantities describing the microstructural inhomogeneity of particulate reinforced composites ($Ni_{60}Nb_{40}$/Mg). A quantitative parameter as degree of clustering is defined to consider particle clustering effect. The results indicate that the damage growth rate of composite with higher degree of clustering is significantly higher than those composites with lower degree of clustering. The *in-situ* growth behavior of equivalent plastic strains as a new approach provides more detailed information about particle clustering effect on plastic deformation. The dislocation description of deformation in two-phase materials rationalize particle clustering effect on the yield behavior of the particulate reinforced composites and the flow stress in these composites. Results show the macroscopic stresses that lead to the initial yielding in the matrix decrease when clusters closely proximate with bigger size and higher degree of clustering. It is found that for region with higher degree of clustering and bigger size of clusters, the von Mises stress is higher at the same loading condition and the growth rate of von Mises stress is considerably higher than the other region with lower degree of clustering. The regions that clusters located in close proximity are potential sites for debonding and void formation since the hydrostatic stress have peak values and the plastic flow is constrained there.

References

[1] Tszeng TC. The effects of particle clustering on the mechanical behavior of particle reinforced composites. Composites: Part B 1998;29:299–308.

[2] Mishnaevsky L, Derrien K, Baptiste D. Effect of microstructure of particle reinforced composites on the damage evolution: probabilistic and numerical analysis. Compos Sci Technol 2004;64:1805–18.

[3] Segurado J, Llorca J. Computational micromechanics of composites: the effect of particle spatial distribution. Mech Mater 2006;38:873–83.

[4] Ayyar A, Crawford GA, Williams JJ, Chawla N. Numerical simulation of the effect of particle spatial distribution and strength on tensile behavior of particle reinforced composites. Comput Mater Sci 2008;44:496–506.

[5] Peng Z, Fuguo L. Effects of particle clustering on the flow behavior of SiC particle reinforced Al metal matrix composites. Rare Met Mater Eng 2010;39:1525–31.

[6] Nafar Dastgerdi J, Marquis G, Anbarlooie B, Sankaranarayanan S, Gupta M. Microstructure-sensitive investigation on the plastic deformation and damage initiation of amorphous particles reinforced composites, Compos Struct 2016;142:130-139.

[7] Leon L. Mishnaevsky Jr. Automatic voxel-based generation of 3D microstructural FE models and its application to the damage analysis of composites, Mater Sci Eng A 2005;407:11–23.

[8] Eckschlager A, Han W, Bohm HJ. A unit cell model for brittle fracture of particles embedded in a ductile matrixComp. Mater Sci 2002;25:85–91.

[9] Fritzen F, Bohlke T. Periodic three-dimensional mesh generation for particle reinforced composites with application to metal matrix composites. Int J Solid Struct 2011;48:706–718.

[10] Shakoor M, Bernacki M, Bouchard PO. Ductile fracture of a metal matrix composite studied using 3D numerical modeling of void nucleation and coalescence. Eng Fract Mech 2018;189:110–132.

[11] Zhang J, Ouyang Q, Guo Q, Li Z, Fan G, Su Y, Jiang L, Lavernia EJ, Schoenung JM, Zhang D. 3D Microstructure-based finite element modeling of deformation and fracture of SiCp/Al composites. Compos Sci Technol 2016;123:1-9.

[12] Wang YB, Liu ZG, Liu N, Hu L, Wei YC, Ou JJ. A new geometric modelling approach for 3D braided tubular composites base on Free Form Deformation. Compos Struct 2016;136:75–85.

[13] Shiganga A, Dainingb F, Rujieb H, Yongma P. Effect of manufacturing defects on mechanical properties and failure features of 3D orthogonal woven C/C composites, Composites: Part B 2015;71:113-121.

[14] Zabihzadeh S, Cugnoni J, Duarte LI, Van Petegem S, Van Swygenhoven H. Deformation behavior of nano-porous polycrystalline silver. Part II: Simulations, Acta Materialia 2017;131: 564-573.

[15] Chen Z, Wang W, Giuliani F, Atkinson A. Analyses of microstructural and elastic properties of porous SOFC cathodes based on focused ion beam tomography, J. Power Sources 2015;273: 486e494.

[16] Mayer CR, Molina-Aladareguia J, Chawla N. Three dimensional (3D) microstructure-based finite element modeling of Al-SiC nanolaminates using focused ion beam (FIB) tomography, Mater Charact 2016;120:369–376.

[17] Yang Z, Ren W, Sharma R, McDonald S, Mostafavi M, Vertyagina Y, Marrow TJ. In-situ X-ray computed tomography characterisation of 3D fracture evolution and image-based numerical homogenisation of concrete, Cement Concrete Compos 2017;75:74-83.

[18] Knackstedt MA, Arns CH, Saadatfar M, Senden TJ, Limaye A, Sakellariou A, Sheppard AP, Sok RM, Schrof W, Steininger H. Elastic and transport properties of cellular solids derived from three-dimensional tomographic images, Proc R Soc Lond Math Phys Eng Sci 2006;462:2833-2862.

[19] Carr J, Milhet X, Gadaud P, Boyer SAE, Thompson GE, Lee P. Quantitative characterization of porosity and determination of elastic modulus for sintered micro-silver joints, J Mater Process Technol 2015;225:19-23.

[20] Hardin RA, Beckermann C. Effect of porosity on the stiffness of cast steel, Metall Mater Trans A 2007;38:2992-3006.

[21] Ayadi A, Nouri H, Guessasma S, Roger F. Determination of orthotropic properties of glass fibre reinforced thermoplastics using X-ray tomography and multiscale finite element computation, Comps Struct 2016;136:635–649.

[22] Michailidis N, Stergioudi F, Omar H, Tsipas DN. An image-based reconstruction of the 3D geometry of an Al open-cell foam and FEM modeling of the material response, Mech Mater 2010;42:142-147.

[23] Tserpes KI, Stamopoulos AG, Pantelakis SpG. A numerical methodology for simulating the mechanical behavior of CFRP laminates containing pores using X-ray computed tomography data, Composites: Part B 2016;102:122-133.

[24] Saucedo-Mora L, Mostafavi M, Khoshkhou D, Reinhard C, Atwood R, Zhao S, Connolly B, Marrow TJ. Observation and simulation of indentation damage in a SiC–SiC fibre ceramic matrix composite, Finite Elem Anal Des 2016;110:11–19.

[25] Penumadu D, Kim F, Bunn J. Damage of composite materials subjected to projectile penetration using high resolution X-ray microcomputed tomography, Exp Mech 2016;56(4):607–616.

[26] Naouar N, Vidal-Salle E, Schneider J, Maire E, Boisse P. 3D composite reinforcement meso F.E. analyses based on X-ray computed tomography, Compos Struct 2015;132:1094–1104.

[27] Shigang A, Xiaolei Z, Yiqi M, Yongmao P, Daining F. Finite element modeling of 3D orthogonal woven C/C composite based on micro-computed tomography experiment, Appl Compos Mater 2014;21(4):603–614.

[28] Aravand MA, Shishkina O, Straumit I, Liotta AH, Wicks SS, Wardle BL, Lomov SV, Gorbatikh L. Internal geometry of woven composite laminates with “fuzzy” carbon nanotube grafted fibers, Compos Part A: Appl Sci Manuf 2016;88:295–304.

[29] Quan Z, Larimore Z, Qin X, Yu J, Mirotznik M, Byun JH, Oh Y, Chou TW. Microstructural characterization of additively manufactured multi-directional preforms and composites via X-ray micro-computed tomography, Compos Sci Technol 2016;131:48–60.

[30] Zou C, Marrow TJ, Reinhard C, Li B, Zhang C, Wang S. Porosity characterization of fiber-reinforced ceramic matrix composite using synchrotron X-ray computed tomography, J Instrum 2016;11(03):C03052.

[31] Blacklock M, Shaw JH, Zok FW, Cox BN. Virtual specimens for analyzing strain distributions in textile ceramic composites, Compos Part A: Appl Sci Manuf 2016;85:40–51.

[32] Padilla E, Jakkali V, Jiang L, Chawla N. Quantifying the effect of porosity on the evolution of deformation and damage in Sn-based solder joints by X-ray microtomography and microstructure-based finite element modeling, Acta Materialia 2012;60:4017–4026.

[33] Chawla N, Sidhu RS, Ganesh VV. Three-dimensional visualization and microstructure-based modeling of deformation in particle-reinforced composites, Acta Materialia 2006;54:1541–1548.

[34] Maire E, Fazekas A, Salvo L, Dendievel R, Youssef S, Cloetens P, et al. X-ray tomography applied to the characterization of cellular materials. Related finite element modeling problems. Compos Sci Technol 2003;63:2431-2443.

[35] Yu J, Zhou C, Zhang H. A micro-image based reconstructed finite element model of needle-punched C/C composite, Compos Sci Techno 2017;153:48-61.

[36] Li Y, Sun B, Gu B. Impact shear damage characterizations of 3D braided composite with X-ray micro-computed tomography and numerical methodologies, Compos Struct 2017;176:43–54.

[37] Lewandowski JJ, Liu C, Hunt WH. Effects of matrix microstructure and particle distribution on fracture of an aluminum metal matrix composite. Mater. Sci. Eng. A 1989;107:241–255.

[38] Cantwell WJ, Roulin-Moloney AC. Fractography and failure mechanisms of unfilled and particulate filled epoxy resins. In: Fractography and Failure Mechanisms of Unfilled and Particulate Filled Epoxy Resins. 1989;234–289.

[39] Hong SJ, Kim HM, Huh D, Suryanarayana C, Chun BS. Effect of clustering on the mechanical properties of SiC particulate-reinforced aluminum alloy 2024 metal matrix composites. Mater Sci and Eng A 2003;347:198–204.

[40] Borbely A, Biermann H, Hartmann O. FE investigation of the effect of particle distribution on the uniaxial stress–strain behaviour of particulate reinforced metal-matrix composites. Mater Sci Eng A 2001;313:34–45.

[41] Deng X, Chawla N. Modeling the effect of particle clustering on the mechanical behavior of SiC particle reinforced Al matrix composites. J Mater Sci 2006;41:5731–5734.

[42] Nafar Dastgerdi J, Miettinen A, Parkkonen J, Remes H. Multiscale microstructural characterization of particulate-reinforced composite with non-destructive X-ray micro- and nanotomography. Compos Struct 2018;194:292–301.

[43] Kak AC, Slaney M, Principles of computerized tomographic imaging, IEEE Press, 1988.

[44] Phansalkar N. et al. Adaptive local thresholding for detection of nuclei in diversity stained cytology images. International Conference on Communications and Signal Processing (ICCSP) 2011, 218-220.

[45] Welzl E. Smallest enclosing disks (balls and ellipsoids), New Results and New Trends in Computer Science (H. Maurer, Ed.), Lecture Notes in Computer Science 1991;555:359-370.

[46] Ashby MF, Kelly A, Nicholson RB. editors. Strengthening methods in crystals. Amsterdam: Elsevier;1971:137–92.

[47] Scudino S, Liu G, Prashanth KG, Bartusch B, Surreddi KB, Murty BS, Eckert J. Mechanical properties of Al-based metal matrix composites reinforced with Zr-based glassy particles produced by powder metallurgy. Acta Mater 2009;57:2029–2039.

[48] Angers R, Krishnadev MR, Tremblay R, Corriveau JF, Dube D. Characterization of SiC_p/2024 aluminum alloy composites prepared by mechanical processing in a low energy ball mill. Mater Sci Eng A 1999;262:9–15.

[49] Arsenault RJ, Fisher RM. Microstructure of fiber and particulate SiC in 6061 Al composites. Scr Metall 1983;17:67–71.

[50] Miller WS, Humphreys FJ. Strengthening mechanisms in particulate metal matrix composites. Scr Metall Mater 1991;25:33–38.

[51] Babaghorbani P, Nai SML, Gupta M. Development of lead-free Sn-3.5Ag/SnO_2 nanocomposites solders. J Mater Sci: Mater Electon 2009;20:571–576.

[52] Brown LM, Stobbs WM. The work hardening of copper-silica v. equilibrium plastic relaxation by secondary dislocations. Philos Mag 1976;34:351–372.

[53] Ashby MF, The deformation of plastically non-homogeneous materials. Philos Mag 1970;21:399-424.

[15] Nafar Dastgerdi J, Marquis G, Anbarlooie B, Sankaranarayanan S, Gupta M, Microstructure-sensitive investigation on the plastic deformation and damage initiation of amorphous particles reinforced composites, Compos Struct 2016;142:130-139.